

Diamond Beam-Position Monitor for Undulator Radiation and Tests at the Tristan Super Light Facility

H. Sakae,^{a,b} H. Aoyagi,^c M. Oura,^a H. Kimura,^c T. Ohata,^c H. Shiwaku,^a S. Yamamoto,^d H. Sugiyama,^d K. Tanabe,^e K. Kobashi^f and H. Kitamura^a

^aSPRING-8, Kamigori, Ako-gun, Hyogo 678-12, Japan, ^bIshikawajima-Harima Heavy Industries Company Ltd, Shin-Nakahara-cho, Isogo-ku, Yokohama 235, Japan, ^cJapan Synchrotron Radiation Research Institute, Kamigori, Ako-gun, Hyogo 678-12, Japan, ^dPhoton Factory, National Laboratory for High Energy Physics, 1-1 Oho, Tsukuba-shi 305, Japan, ^eSumitomo Electric Industries Ltd, 1-1-1 Koya-kita, Itami, Hyogo 664, Japan, and ^fKobe Steel Ltd, 5-5 Takatukadai 1-chome, Nishi-ku, Kobe, Hyogo 651-22, Japan. E-mail: hisaharu_sakae@ihi.co.jp

(Received 31 May 1996; accepted 11 April 1997)

A photon beam-position monitor using a diamond foil as a position-sensitive device has been developed for use on insertion-device beamlines of third-generation synchrotron radiation facilities such as SPRING-8, and was tested on the undulator beamline of the Tristan Super Light Facility at KEK. The beam test results show that the diamond monitor can be operated in a photoconductive mode like a semiconductor detector. It has a linear working range of about ± 1 mm and a position sensitivity of less than $3 \mu\text{m}$. The stability of the monitor was confirmed by continuous operation under low photon beam intensity conditions.

Keywords: beam-position monitors; diamond; photoconductive mode; undulator radiation.

1. Introduction

With the advances in user experiments using synchrotron light sources, accurate control and a stable supply of the photon beam have become indispensable. Therefore, a photon beam-position monitor with a high position sensitivity of less than a few micrometres and stability under high heat load is required. Blade-type monitors utilizing photoelectron emission have been conventionally used for insertion-device beamlines. However, they will not be able to withstand the extremely high thermal loads of third-generation synchrotron sources such as SPRING-8 because the maximum total power and density of undulator radiation will reach about 11 kW and 470 kW mrad^{-2} , respectively. Moreover, the following problems inherent to this type of monitor have become apparent (Loyer, 1993):

- (i) contamination of undulator radiation by radiation from adjacent bending magnets;
- (ii) drift of the measured position induced by the change of the undulator gap;
- (iii) shadowing effect of the upstream beam-position monitor on the downstream beam-position monitor.

As a candidate for a beam-position monitor which satisfies these requirements and solves these problems we have been developing a position-sensitive device using a diamond foil which is operated in a photoconductive mode. The prototype monitor was tested on the MR-BW-TL beamline of the Tristan Super Light Facility (Ando & Kikuta, 1995) at KEK. The design of the monitor and results from the beam tests are presented in this paper.

2. Diamond monitor

2.1. Principle of operation

The principle of operation of the diamond monitor is shown in Fig. 1. Electrodes are positioned on both sides of a diamond foil and an external voltage is applied between the electrodes to produce an electric field in the diamond. When the photon beam irradiates the diamond, free carriers (electrons and holes) are created by the interaction of photons with the diamond. These carriers drift along the electric field and generate a current in the external circuit (Knoll, 1989). The photoconductive signal of the monitor is proportional to the radiation power absorbed in the diamond. The sensitivity to hard X-rays is emphasized in comparison with a photoelectron-emission-type monitor that has a high sensitivity to UV and soft X-rays. Therefore, contamination by the soft X-ray background radiation from bending magnets and the drift of the measurement brought by it are expected to be reduced.

As shown in Fig. 2 the electrodes of the prototype monitor are segmented into four parts in order to obtain information on the two-dimensional beam position. With the currents from each electrode the beam centroid can be found using the following formulae:

$$X = A_x \frac{[(I_{U-R} + I_{D-R}) - (I_{U-L} + I_{D-L})]}{[(I_{U-R} + I_{D-R}) + (I_{U-L} + I_{D-L})]}, \quad (1)$$

$$Y = A_y \frac{[(I_{U-R} + I_{U-L}) - (I_{D-R} + I_{D-L})]}{[(I_{U-R} + I_{U-L}) + (I_{D-R} + I_{D-L})]}, \quad (2)$$

where I_{U-R} , I_{U-L} , I_{D-R} , I_{D-L} (U : upper, D : down, R : right,

L : left) are currents from each electrode and A_x , A_y are calibration coefficients.

The superior thermophysical properties of diamond, such as high thermal conductivity, low thermal expansion, high mechanical stiffness and radiation hardness, make it possible to be used in the harsh environment at the front end of beamlines where other semiconductor detectors cannot be used. The electric properties of diamond are shown in Table 1 along with those of silicon. Moreover, the following advantages make diamond an attractive candidate as a photon beam-position monitor (Franklin *et al.*, 1992):

(i) the high saturated carrier velocity produces a quick response;

Table 1

Electric properties of diamond and silicon.

Property	Diamond	Silicon
Band gap (eV)	5.5	1.1
Resistivity (Ω cm)	$>10^{12}$	2×10^5
Electron mobility ($\text{cm}^2 \text{V}^{-1} \text{s}^{-1}$)	1800	1500
Hole mobility ($\text{cm}^2 \text{V}^{-1} \text{s}^{-1}$)	1200	500
Saturation velocity ($\mu\text{m ns}^{-1}$)	220	100
Dielectric constant	5.6	11.7
Energy to create electron-hole pair (eV)	13	3.6
Mass density (g cm^{-3})	3.5	2.3
Average minimum ionizing particle signal per 100 μm (electrons)	3600	8000
Average minimum ionizing particle signal per 0.1% X_0 (electrons)	4500	7500

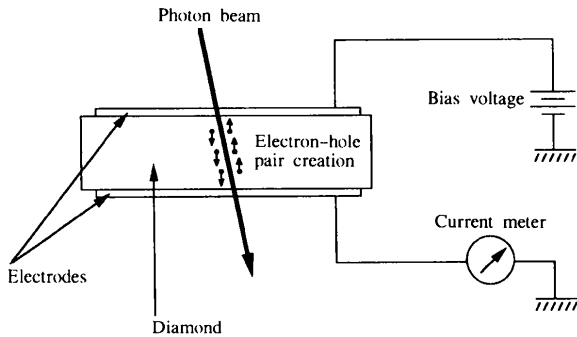


Figure 1
Principle of the diamond monitor operation.

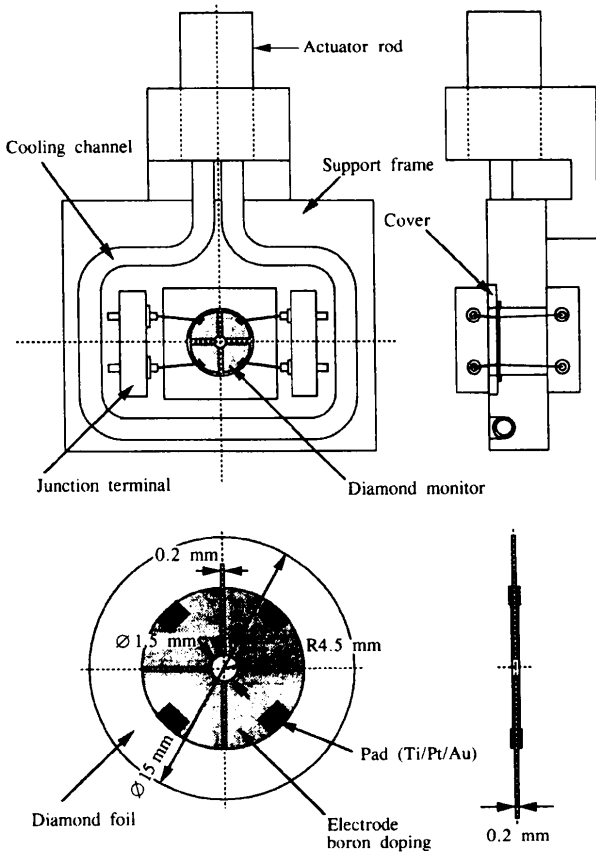


Figure 2
Schematic view of the diamond monitor operation.

(ii) the low capacitance realizes the high signal-to-noise ratio;

(iii) the low leak current due to high resistivity enables a simple structure with no need for a reverse biased $p-n$ junction;

(iv) the large band gap reduces the sensitivity to visible radiation.

2.2. Structure

A schematic view of the diamond monitor is shown in Fig. 2. A synthetic polycrystalline diamond film, which was made by the chemical vapour deposition (CVD) process, was used as an active element (the diamond foil was manufactured by Sumitomo Electric Industries, Ltd). The light element as a diamond provides a high transmission of X-rays; therefore, shadowing effects are expected to be prevented and the heat load will be also reduced. The size of the diamond is $\text{\O}15 \text{ mm} \times 0.2 \text{ mm}$ and its measured resistivity is $\sim 10^{12} \Omega \text{ m}$. For better transmission of X-rays and reduction of the heat load the diamond has a hole of diameter 1.5 mm in the centre. The diameter corresponds to the FWHM of the horizontal power distribution of the standard undulator radiation of SPring-8. Four electrodes were symmetrically formed on each surface of a diamond foil by heavy doping of boron. Doping of a light element such as boron reduces the X-ray absorption in comparison with a metal electrode using Au or Al. Although the CVD diamond tends to have many grain boundaries and structural defects near the surfaces, these defects can be eliminated by forming low resistive layers, also by heavy doping of boron.

Electrodes on one side were ganged by wires and biased to a common voltage, while those on the other side were connected to each signal line. The connection between the electrodes and the signal lines was made with wire bonding. For firm bonding, small pads made of Ti/Pt/Au were plated on the electrodes. The diamond was clamped onto a support frame by a copper cover. A thin Au foil was placed between the diamond and the support frame to achieve a good thermal conductance. The diamond was indirectly cooled through the copper frame onto which a water-cooling pipe was brazed. Two thermocouples were attached to the frame for monitoring the temperature of the diamond.

3. Experimental arrangement

3.1. Beamline

The MR-BW-TL beamline (*Photon Factory Activity Report*, 1994, 1995) is a highly brilliant undulator beamline constructed in the Tristan main ring and remodelled in order to attain a very low emittance of a few nm rad at 10 GeV.

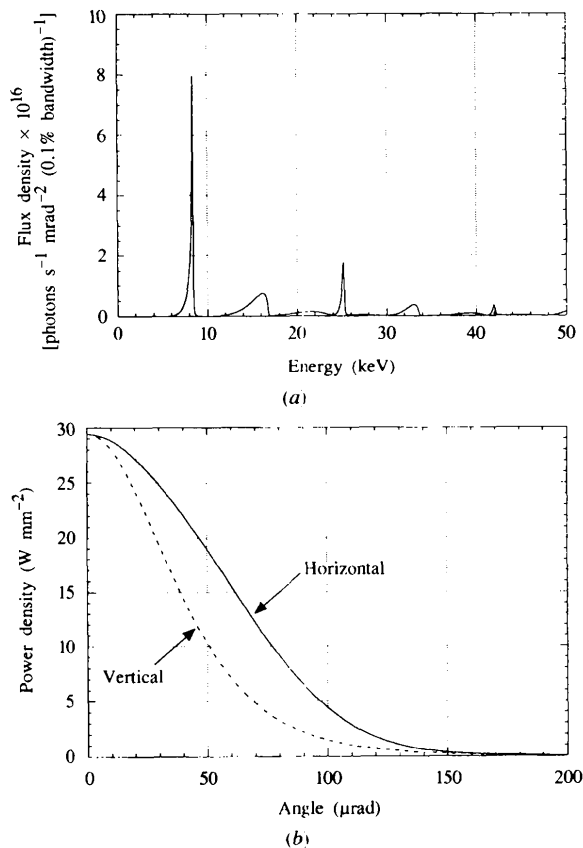


Figure 3
(a) Spectral flux of the radiation from the undulator calculated using the parameters $\lambda_u = 45$ mm, $N = 120$, $K = 1.1$. The beam energy is 8 GeV and the beam current is 10 mA. (b) Angular power density distribution of the undulator radiation at the monitor position.

Table 2

Tristan main ring and undulator parameters.

Main ring	
Electron energy	10 GeV/8 GeV
Beam current	~10 mA (8-bunch mode) ~16 mA (32-bunch mode)
Emittance	5 nm rad (design value at 10 GeV)
Undulator	
Magnetic length	5.4 m
Number of period	120
Period length	45 mm

The undulator is a planar type with a pure configuration of permanent magnets (Yamamoto, Shioya, Kitamura & Tsuchiya, 1995). Typical parameters of the main ring and the undulator are shown in Table 2.

Monitor data were taken under conditions where the beam energy was 8 GeV, the beam current was $\sim 30 \mu\text{A}$ –5 mA and the K value of the undulator was about 1.1, which gave a fundamental photon energy of 8.4 keV. The simulated spectral flux of the undulator radiation (Kitamura, 1994) at a beam current of 10 mA is shown in Fig. 3(a). The total radiated power is 150 W and the maximum power density at the monitor position reaches 29 W mm^{-2} as shown in Fig. 3(b). The beam monitor was installed in an ultra-high vacuum portion of the beamline at 20 m from the undulator in order to test its performance under high vacuum and high-heat-load conditions.

3.2. Experimental set-up

The experimental set-up for the monitor test is shown in Fig. 4. The vacuum vessel for the monitor was equipped with a linear actuator, which was driven by a stepping motor, for vertical motion of the monitor, and the vessel was mounted on an X stage for horizontal motion. The minimum stepping size in both directions was $0.1 \mu\text{m}$. The monitor and adjacent apparatus were joined through welded bellows. The four current signals of the monitor were sequentially fed into the electrometer *via* a scanner card and were digitized.

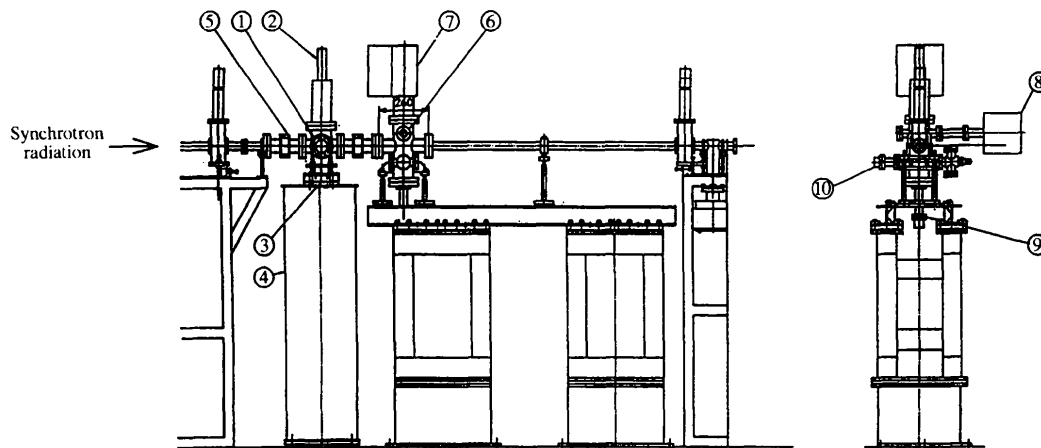


Figure 4
Experimental set-up for the monitor test. (1) Vacuum vessel; (2) linear actuator; (3) X stage; (4) base structure of carbon-fibre-reinforced plastic; (5) bellows; (6) vacuum vessel for pumping; (7) ion pump; (8) gas analyzer; (9) titanium getter pump; (10) ion gauge.

The monitor was mounted on a base structure of carbon-fibre reinforced plastic (manufactured by Nippon Oil Company Ltd). The linear expansion coefficient in the vertical direction was designed to be nearly zero by adjusting the fibre angle between each staking laminate of the carbon-fibre reinforced plastic. The height variation caused by an environmental temperature change of about ± 1 K could be reduced to within $1 \mu\text{m}$. The size of the base structure was $\varnothing 376 \times 1275$ mm. The vacuum system, which consisted of a vacuum vessel, ion pump (1251 s^{-1}), titanium getter pump (10001 s^{-1}), residual gas analyzer and ion gauge, was placed downstream of the monitor.

4. Results

4.1. Signal properties

The signal currents from each electrode of the monitor as a function of the bias voltage applied to the diamond when the photon beam passed through the centre of the monitor are shown in Fig. 5. The beam current was $30 \mu\text{A}$ and the K value of the undulator was 1.05. The signal current increased and became saturated with the increase of the bias voltage. The current direction was changed in accordance with the polarity of the applied voltage. Because the current direction cannot change in the case of photoelectron emission, the photoconductive current is supposed to flow through the diamond. The signal saturation can be explained by the effect of the drift velocity saturation of free carriers (electrons and holes) in the diamond.

The beam current dependence on the signal current is shown in Fig. 6, where the solid line shows the signal current with a bias voltage of $+10$ V and the dashed line shows the photoelectron current without bias voltage. The signal current increased linearly with the beam current in both cases. Because the photoconductive current is proportional to the power absorbed in the diamond, a large signal current was expected to be generated in the bias-applied case and a current of about two to three orders larger than the photoelectron current was observed. These facts,

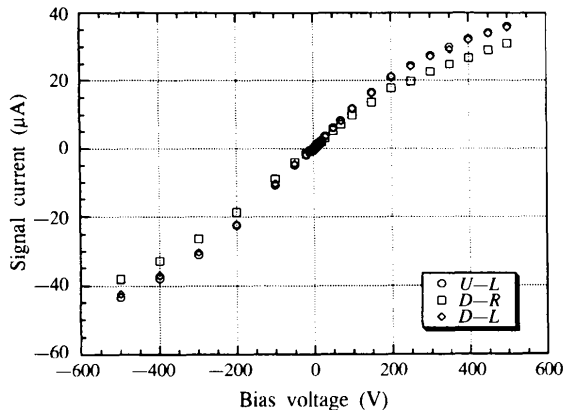


Figure 5
Signal current from each electrode of the monitor as a function of bias voltage. Beam energy = 8 GeV, beam current = $30 \mu\text{A}$, $K = 1.05$.

i.e. the very large signal, the change of the current direction and the signal saturation, show that the monitor operated in the photoconductive mode when the bias voltage was applied to the diamond. Photoelectron emission occurs even in the photoconductive mode. Therefore, a small amount of the photoelectron current is included in the signal current.

4.2. Sensitivity to the beam motion

For calibration of the monitor the current signal was measured by moving the monitor across the beam in horizontal and vertical directions. The signal current in the photoconductive mode as a function of the beam position for vertical scans is shown in Fig. 7(a). The bias voltage was -25 V and the beam current was 0.15 mA. Those for the photoelectron mode without bias voltage are shown in Fig. 7(b). The beam-position dependence on the signal current was slightly different between the two modes. This was due to the difference in the sensitivity dependence between the two modes on the photon beam energy. The calibration curves for the horizontal and vertical directions, which are the normalized differential currents as a function of the beam position, are shown in Figs. 8(a) and 8(b) for the horizontal and vertical scans, respectively, when the monitor was operated in the photoconductive mode. When the monitor was moved through the acceptable range in this scan the photon beam directly irradiated a cable attached to one electrode (I_{U-R}) and it was broken. Therefore, the following formulae were used instead of equations (1) and (2) to calculate the calibration curve assuming that the photon beam had a bilateral symmetrical shape about the vertical and horizontal beam axes,

$$X = A_x(I_{D-R} - I_{D-L})/(I_{D-R} + I_{D-L}), \quad (3)$$

$$Y = A_y(I_{U-L} - I_{D-L})/(I_{U-L} + I_{D-L}). \quad (4)$$

The calibration curves corresponding to each scan direction

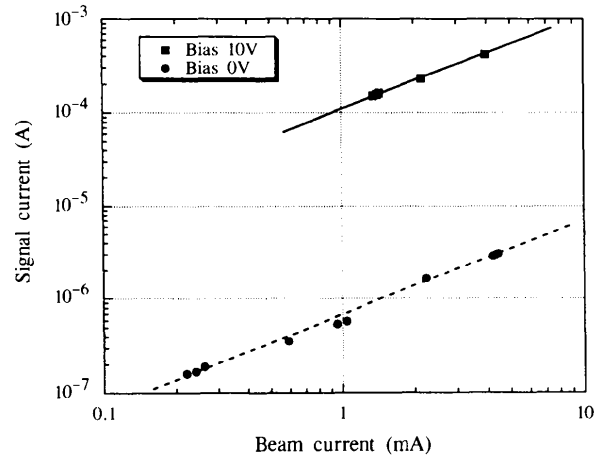


Figure 6
Signal current of the monitor as a function of beam current for $K = 1.1$ and beam operation at 8 GeV. The solid fitted line shows the signal current in the photoconductive mode with a bias voltage of 10 V and the dashed fitted line shows the signal current in the photoelectron mode without bias voltage.

have adequate linear working ranges and axial symmetrical shapes, which shows the availability of the monitor for beam-position measurement and the propriety of the beam-shape assumption. The linear working ranges, where the linearity error is within 10%, are $X = \pm 0.9$ mm and $Y = \pm 0.95$ mm for both operating modes. Calibration coefficients (A_x, A_y) which correspond to the sensitivity to the beam movement are

photoconductive mode: $A_x = 1.37$ mm, $A_y = 1.26$ mm;
 photoelectron mode: $A_x = 1.38$ mm, $A_y = 1.27$ mm.

Fig. 9 shows the results of the scan measurements performed with a $10 \mu\text{m}$ step for the vertical scan when the monitor was operated in the photoconductive mode with a bias voltage of 10 V. The clear jumps of the position signal at each step ensure that the monitor had a position sensitivity of about $3 \mu\text{m}$. Because the fluctuation of the beam during the measurement and the time difference between each sequential reading of signals give additional errors, the monitor is expected to have better position sensitivity in practice.

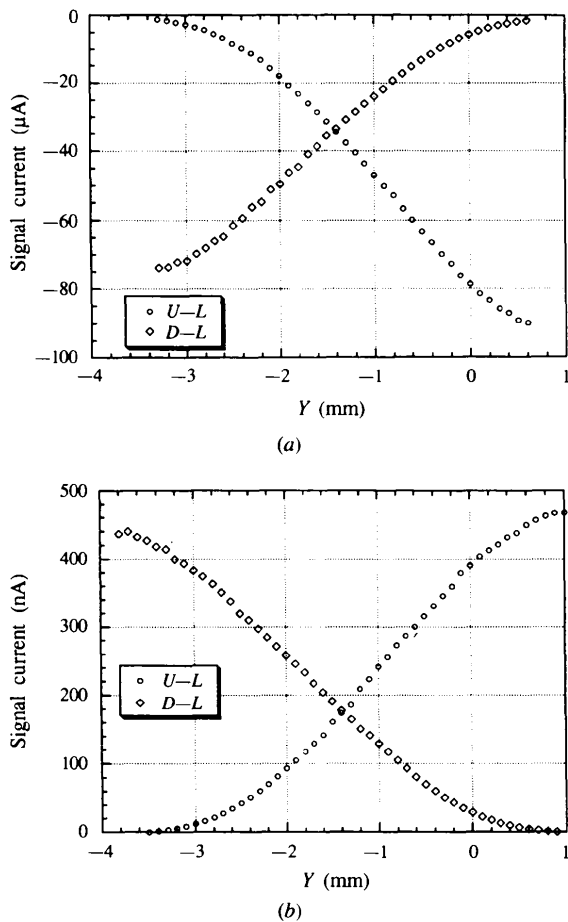


Figure 7
 (a) Signal current of the monitor as a function of beam position for a vertical scan in the photoconductive mode with a bias voltage of -25 V. Beam energy = 8 GeV, beam current = 0.15 mA, $K = 1.07$.
 (b) Signal current of the monitor as a function of beam position for a vertical scan in the photoelectron mode without bias voltage. Beam energy = 8 GeV, beam current = 0.25 mA, $K = 1.07$.

4.3. Stability test

To evaluate the stability of the diamond monitor the photon beam had been monitored in continuous operation during a single stored beam period of 6 h. The beam energy

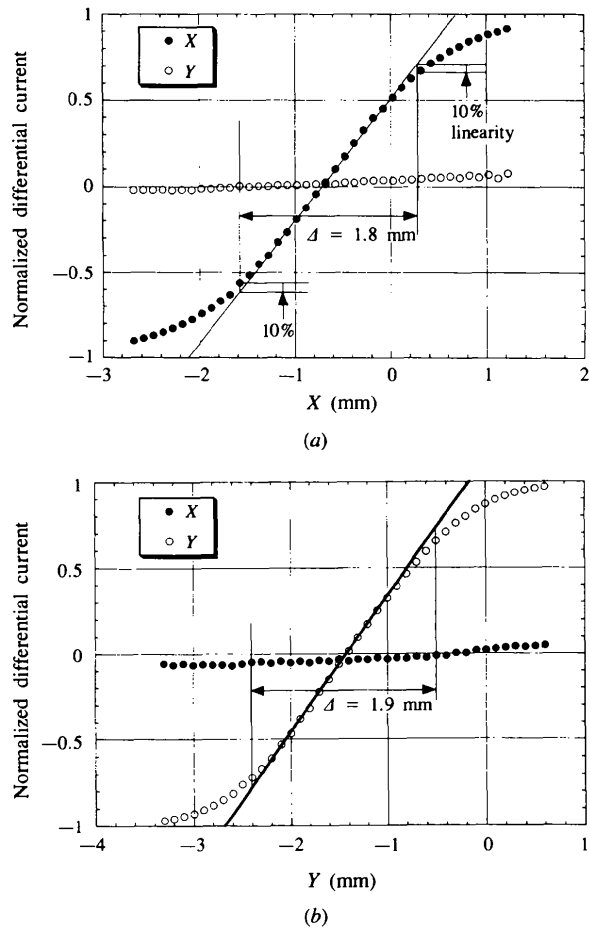


Figure 8
 (a) Calibration curve of the monitor for horizontal movement of the beam. The monitor was operated in the photoconductive mode with a bias voltage of -25 V. (b) Calibration curve of the monitor for vertical movement of the beam. The monitor was operated in the photoconductive mode with a bias voltage of -25 V.

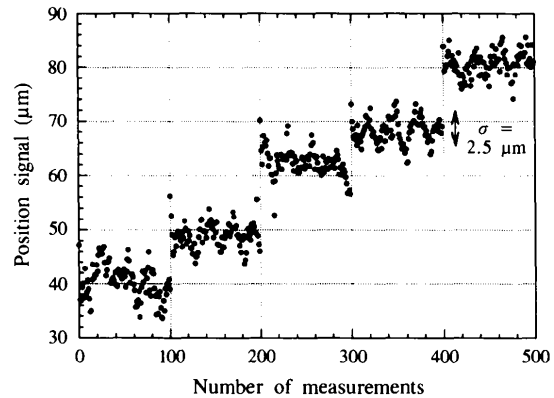


Figure 9
 Scan measurement for a vertical scan performed with a $10 \mu\text{m}$ step. The monitor was operated in the photoconductive mode with a bias voltage of 10 V. Beam energy = 8 GeV, beam current = 1.15 mA, $K = 1.1$.

was 8 GeV and the K value of the undulator was 1.1. The wire monitor (Zhang, Sugiyama, Ando, Xia & Shiwaku, 1995), located 30 m downstream from the diamond monitor, had been operated simultaneously as a reference. The initial position of the diamond monitor was set as the beam passed through the centre of the monitor, while the wire monitor was set at the position of half maximum of the signal current. Fig. 10 shows the historical profile of the signal currents of the diamond monitor and the wire monitor; the beam current is also shown. The signal currents of both monitors decreased in proportion to the beam current, which varied from 130 to 50 μA , and no significant degradation of the monitor could be seen during the operation period. Fig. 11 shows the horizontal beam positions measured by the diamond monitor and the signal currents of the wire monitor normalized by the beam current. Assuming that the beam shape remained constant independently of the beam current, the variation of the normalized signal current of the wire monitor corresponds to that of the beam position. As shown in this figure, both monitors show the same tendencies of beam movements and stable operation.

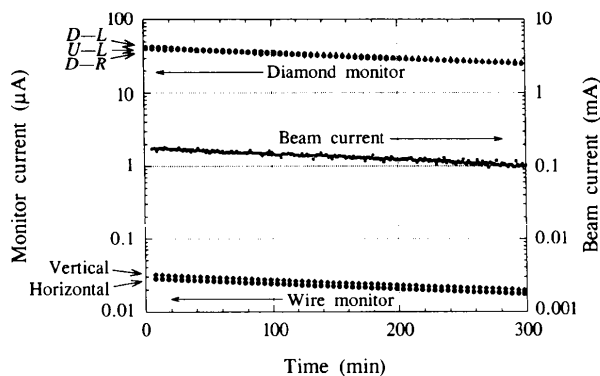


Figure 10

Historical profile of the signal current of the diamond monitor and wire monitors; the beam current is also shown. Beam energy = 8 GeV, $K = 1.1$.

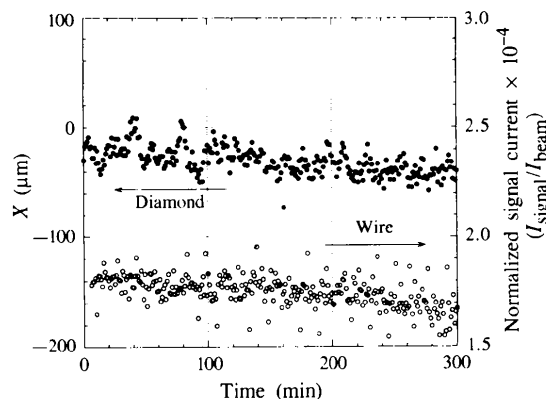


Figure 11

The horizontal beam position measured by the diamond monitor and the signal current of the wire monitor, which is normalized by the beam current.

5. Conclusions

The beam test results show that the photon beam-position monitor using a polycrystalline CVD diamond foil as a position-sensitive device can be operated in the photoconductive mode. In the photoconductive mode the sensitivity to X-rays is higher than that in the photoelectron mode because the photoconductive current is proportional to the absorbed power in the diamond. Owing to enhancement of the sensitivity to hard X-rays, the effect of the background radiation from bending magnets, which disturbs the measurement of the undulator beam position, is expected to be reduced. The monitor has a linear working range of about ± 1 mm and a position sensitivity of less than 3 μm . In continuous operation the monitor was operated stably and no significant degradation could be seen. The monitor is a suitable candidate for the photon beam monitor of third-generation synchrotron radiation facilities by virtue of the superior thermophysical, optical and electrical properties of the diamond foil.

The authors would like to thank the staff of Tristan and the Tristan Super Light Facility for their support during the experiments and valuable advice, especially from M. Ado of KEK. Thanks are also due to Y. Sugimoto of KEK for theoretical advice about the diamond monitor and to M. Mihara of RIKEN for technical advice and help in the bonding of the diamond. Many thanks are due to U. Furukawa, Y. Komura, M. Kuroda, Y. Oikawa and S. Takahashi of RIKEN for their kind help in the preparation for the experiments and the installation of the diamond monitor.

References

- Ando, M. & Kikuta, A. (1995). *J. Phys. Soc. Jpn*, **50**, 15–20. (In Japanese.)
- Franklin, M., Fry, A., Gan, K. K., Han, S., Kagan, H., Kanda, S., Kania, D., Kass, R., Kim, S. K., Malchow, R., Morrow, F., Olsen, S., Palmer, W. F., Pan, L. S., Sannes, F., Schnetzer, S., Stone, R., Sugimoto, Y., Thomson, G. B., White, C. & Zhao, S. (1992). *Nucl. Instrum. Methods*, **A315**, 39–42.
- Kitamura, H. (1994). *SPECTRA. Synchrotron Radiation Calculation Program for PC98*. SPring-8, Kamigori, Ako-gun, Hyogo, Japan.
- Knoll, G. F. (1989). *Radiation Detection and Measurement*. New York: Wiley.
- Loyer, F. (1993). *Proc. DIPAC'93*. Montreux, Switzerland.
- Photon Factory Activity Report* (1994). No. 11, S-1. Photon Factory, National Laboratory for High Energy Physics, Tsukuba-shi, Japan.
- Photon Factory Activity Report* (1995). No. 12, P-1. Photon Factory, National Laboratory for High Energy Physics, Tsukuba-shi, Japan.
- Yamamoto, S., Shioya, T., Kitamura, H. & Tsuchiya, K. (1995). *Rev. Sci. Instrum.* **66**, 1996–1998.
- Zhang, X., Sugiyama, H., Ando, M., Xia, S. & Shiwaku, H. (1995). *Rev. Sci. Instrum.* **66**, 1990–1992.